Fermilab Italian summer student program 2023

The ICARUS light detection system

Leo Mareso

Supervisors:
Donatella Torretta, Gian Luca Raselli

Abstract

The ICARUS T600 detector is the largest Liguid Argon Time Projection Chamber ever used on a neutrino beam, and it acts as the far detector of the Short Baseline Neutrino program at Fermilab. Its purpose is the study of the possibility of the existence of a fourth sterile neutrino in the O(eV^2) mass range that could take part in the neutrino oscillations. The light detection system of the ICARUS detector plays the role of localising in space and time the neutrino interactions taking place inside the detector, collecting the argon scintillation photons generated when an event occurs. This light detection system also has a crucial role in the trigger system and the rejection of the huge amount of background cosmic events, working together with the trigger request signals sent by the beam complex. In August 2023 part of the cables that are used to carry the signals from the photomultipliers to the electronics were replaced with a new model, because a deterioration of the quality of the signal inside the cables had previously been observed. An analysis of the performance of the new cables was carried out, comparing laser run data collected before and after the change of the cable model, and it was proved that the introduction of the new cables lead to a general improvement of the quality of the signals reaching the electronics.

Special thanks to Matteo Vincenzi for helping me out whenever I had any kind of software related problem.

Contents

Introduction

The ICARUS T600 experiment is a LAr-TPC detector now operating at Fermilab to confirm or reject the possibility of the existence of a fourth sterile neutrino in the O(eV^2) mass scale. In August 2023 the signal cables connecting the PMTs in the West cryostat to the electronics were replaced with new signal cables to better preserve the shape of the signal reaching the electronics. *Section 1* will give a brief theoretical context on the subject, followed by *Section 2* which will give an overview of the SBN program and ICARUS experiment at Fermilab. The ICARUS detector and its light detection system will be discussed more in detail in *Section 3*. *Section 4* explains the electronics and the data acquisition of the light detection system. *Section 5* will be dedicated to the analysis of the data gathered using the new signal cables comparing them to the old ones.

1 Neutrino and neutrino oscillations

Neutrinos are lepton particles in the standard model which do not have electromagnetic nor strong interactions, therefore they are chargeless for both interactions. There are three "active" interacting neutrinos in the standard model, one for each charged lepton particle (e, μ, τ), and each neutrino can interact through Charged Current (CC) interactions involving the corresponding charged lepton or by means of Neutral Current (NC) interactions when they only involve themselves. Measurements on the decay width of the Z^0 boson imply the existence of three and only three light active neutrinos in the standard model framework, meaning there are no weakly interacting neutrinos having a mass smaller than $m_{Z^0}/2$. Sterile neutrinos instead are defined as particles not having any standard model gauge interaction, therefore there is no known existing sterile neutrino since the standard model describes all known particle interactions.

In the standard model neutrinos do not have a mass since the leptons would have to interact with the Higgs field in both left and right handed components, but only left-handed neutrinos do, so there is no way to construct a renormalisable mass term in the standard model lagrangian.
However the observation of neutrino oscillations confirmed the massive nature of the known neutrinos. Neutrino oscillations refer to the neutrino property of not conserving its lepton flavor during its propagation, which is a consequence of the fact that neutrino interaction eigenstates and mass eigenstates do not coincide. Considering all three the active neutrinos, the two basis are connected by a mixing matrix U^{PMNS} which regulates the flavour transition probabilities $P_{\alpha\beta}$ of an interacting neutrino ν_α to a different flavour ν_β.

$$|\nu_\alpha(t)\rangle = \sum_{n=1}^{3} U_{\alpha i}^{PMNS} |\nu_i(t)\rangle \tag{1}$$

$$P_{\alpha\beta} = |\langle \nu_\beta | \nu_\alpha(t) \rangle|^2 \tag{2}$$

However recent experiments reported some anomalies in the results which could hint the existence of a fourth sterile neutrino participating in the mixing of the flavours. These anomalies include the reactor anomaly and the Gallium anomaly, where there is a deficit of $\bar{\nu_e}$, and the LSND and MicroBooNE anomalies, having an excess of ν_e and $\bar{\nu_e}$. The introduction of a fourth sterile neutrino in the $\Delta m^2 = 1$ eV^2 mass range could explain both of these phenomena, but there is still no experimental evidence to confirm its existence [1].

2 The SBN Program and the ICARUS detector

The SBN (Short-Baseline Neutrino) Program is a Short-Baseline accelerator neutrino oscillation experiment at Fermilab. It studies neutrino properties and neutrino oscillations using a neutrino beam generated by the 8 GeV

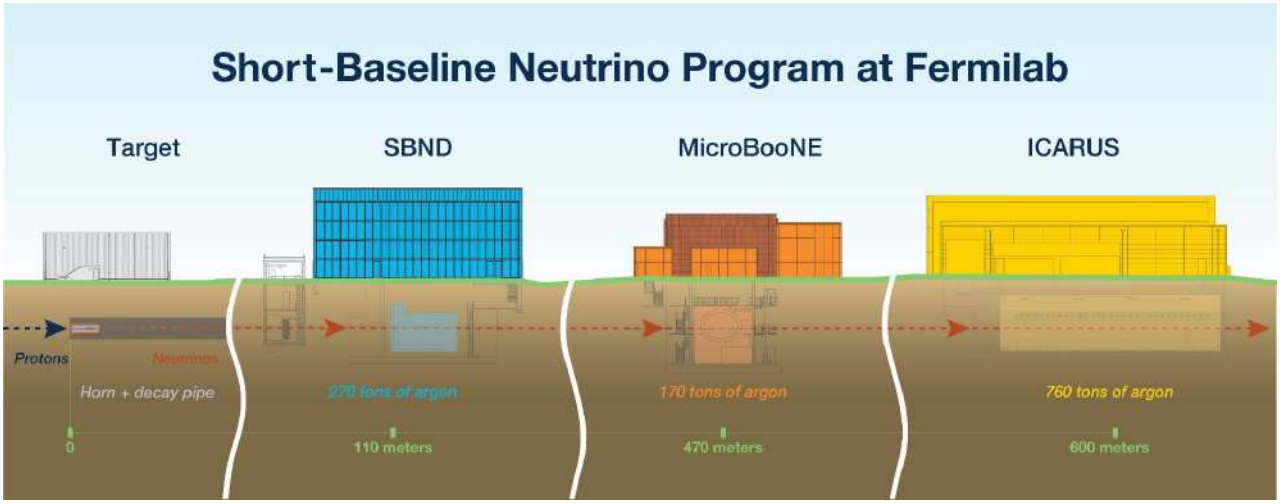

Figure 1: *Diagram explaining the structure of the SBN program at Fermilab [2].*

protons accelerated in the Booster accelerator (Booster Neutrino Beam, BNB) and measuring its flux and its energy spectrum along the axis on a relatively short distance [1, 3].
The probability $P_{\alpha\beta}$ of a neutrino to change its flavor in an interaction in the 2-flavor oscillation limit is given by:

$$\begin{aligned} P_{\alpha\beta} &= P(\nu_\alpha \to \nu_\beta) \\ &= \delta_{\alpha\beta} - (2\delta_{\alpha\beta} - 1) sin^2(2\theta) sin^2\left(\frac{\Delta m^2 L}{4E}\right) \\ &\overset{\alpha\neq\beta}{=} sin^2(2\theta) sin^2\left(\frac{\Delta m^2 L}{4E}\right) \\ &= sin^2(2\theta) sin^2\left(1.267 \frac{\Delta m^2 L}{E} \frac{MeV}{eV^2 m}\right) \end{aligned} \tag{3}$$

where θ is the mixing angle of the two flavors, Δm^2 is the square difference of the two neutrino mass eigenvalues, L is the distance between the production point and the interaction point of the neutrino and E is the energy of the neutrino [4]. In order to be able to observe and study neutrino oscillations the argument of the second sine function must be O(1).
A Short-baseline neutrino oscillation experiment has typical values of the order of $L = \mathrm{O}(10^2\ \mathrm{m})$, $E = \mathrm{O}(\mathrm{GeV})$ so that it can study oscillations in the mass range of $\Delta m^2 = \mathrm{O}(\mathrm{eV}^2)$ [4].
The experiment consists of three large Liquid Argon Time Projection Chamber (LAr-TPC) detectors located along the axis of the BNB in a way such that the sensitivity of the oscillations is optimised and the impact of the systematic uncertainty of the flux is minimised [1]. *Figure 1* summarises the details of the detectors and of the program. The BNB predominantly consists of muonic neutrinos peaking around 700 MeV and the far detector is located at 600 m from the beam target, therefore exploiting *Equation 3* it's clear that the SBN program meets the characters of a short baseline experiment.
ICARUS T600 is the far detector of the experiment and it is located 600 m far from the target of the beam. It is by far the largest LAr-TPC ever used on a neutrino beam and it contains 760 tons of LAr. The detector consists in two large cryostats, usually referred as the West and East cryostats, each having internal dimensions $3.6 \times 3.9 \times 19.6\ \mathrm{m}^3$. Both modules are split into two TPCs having a drift path of 1.5 m that share a common cathode at -75 kV in the middle, generating an electric field of 500 V/cm in each TPC. Each one of the 4 TPCs contains 3 readout wire planes, of which 2 are induction wires and only 1 is the charge collection anode wire plane, and 90 photomultipliers (PMTs) to detect the LAr scintillation light that occurs when an interaction takes place in the detector [5].

Charged particle tracks in the TPC can be reconstructed by collecting through the wire planes the ionised charges on two dimensions, while the third dimension is given by the drift time of the charges, measured as the time gap between the interaction timing, measured by the PMTs, and the charge collection timing. The main goal of the SBN program and of the ICARUS detector is the study of the possibility of the existence of a fourth sterile neutrino in the O(eV^2) mass range. As mentioned in the previous section, several experimental anomalies pointing at additional physics beyond the standard model in the neutrino sector have been reported in recent years, hinting what could be the existence of an additional neutrino with larger squared mass participating in the mixing.
In addition it also has the purpose to develop the knowledge and technology of large scale LAr-TPC experiments in the GeV energy range for future experiments like DUNE, for example by measuring the cross section of a neutrino with an Argon molecule.
Moreover, ICARUS can also collect data as an off-axis detector from the NuMI (Neutrinos at the Main Injector) beam neutrinos, generated from protons accelerated up to 120 GeV in the Main Injector [1].

3 The ICARUS light detection system

The ICARUS light detection system consists of 360 PMTs located inside the 4 TPCs, as shown in *Figure 2*. The PMTs are sensitive to the LAr scintillation photons produced inside the detector when an interaction with an Argon molecule takes place inside. The system has mainly 3 tasks [6]:

- measure the absolute timing of each interaction inside the detector with a precision of the order of O(ns);
- locate longitudinally the interaction point inside the 20 m long detector with an accuracy better than 1 m;

Figure 2: *Picture of the PMTs mounted on one of the inner walls of the ICARUS TPC [5].*

- take part in the trigger system to select only interesting events and reject the huge amount of cosmic background events.

The PMTs used in the detector are 8" Hamamatsu R5912-MOD devices. The model was chosen after an evaluation comparing it with other PMTs considering several factors, such as the sensitivity to ionising events in LAr down to 100 MeV energy deposition, the tightness of PMT pulses, resistance to cryogenic temperatures and high pressures, the absence of

Figure 3: *Picture of a PMT in its stainless steel cage and an optical fiber pointing towards it [6].*

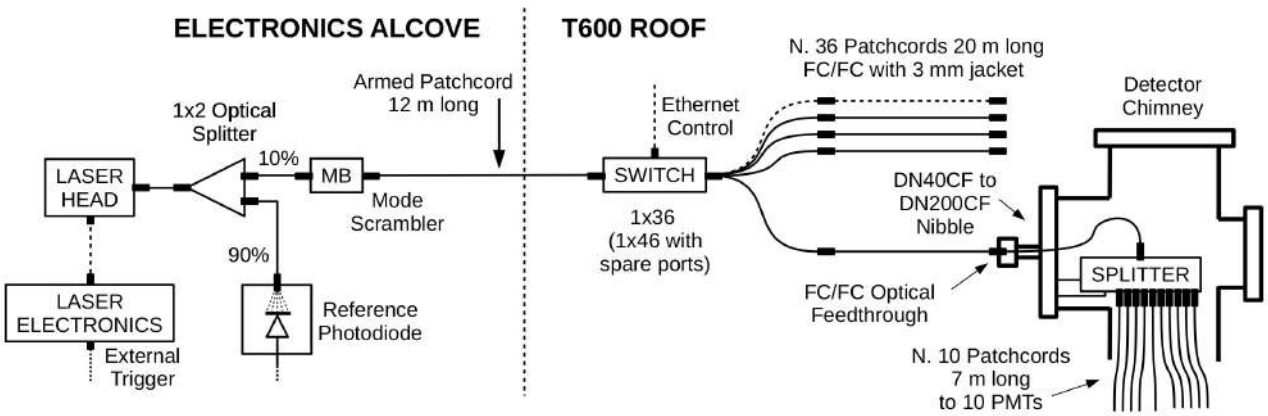

Figure 4: *Diagram of the laser calibration system [6].*

noise generating pulses above the single photon level and other technical factors. Each PMT is covered by a layer 200 μg/cm^2 of Tetraphenyl-Butadiene (TPB), a wavelength shifter. In fact the scintillation photons have a frequency in the Vacuum Ultra Violet (VUV) range, therefore their frequency must be shifted in the visible spectrum since PMT glass windows are not transparent to argon scintillation photons. The coating was applied through specific evaporation precedures involving a thermal evaporator to ensure a high repeatability and reliability of the procedure. To guarantee high performance at cryogenic temperatures, each PMT features an 8" hemispherical glass window with bialkali photocathode on platinum undercoating. The quantum efficiency of the coated PMTs have an average quantum efficiency value of 0.12. [5, 6, 7, 8].
Each PMT is mounted on the inner wall of the TPC, in the 30 cm space behind the wire planes and 5 mm far from them. Moreover grounded stainless steel cages are mounted around every PMT to mitigate the induction of fake signals on the wire that could be caused by the electron multiplication process inside the PMTs, as shown in *Figure 3*. Each PMT is also provided with a laser injection fiber mounted on the cage pointing towards the photocathode. These fibers are part of the laser calibration system of the PMTs, which is useful for the monitoring of the performance of each PMT in the detector and the calibration of their gain, to have them equalised. It consists of a Hamamatsu PLP10 laser diode generating fast laser pulses in the electronics alcove by the detector and a light distribution system sending the pulse signals to every PMT. The laser pulse has a nominal width of 100 ps and a λ of 405 nm. It starts from the laser head and after passing through 50 µm patch cables it reaches an optical switch on the roof of the detector, that splits the signal into 36 20 m long patch cords, each feeding an optical flange on structures over the detector called chimneys. Inside each chimney there is an optical splitter that further splits the pulse into 10 injection fibers deployed along the mechanical frames of the PMTs [5, 6]. A scheme of the laser distribu-

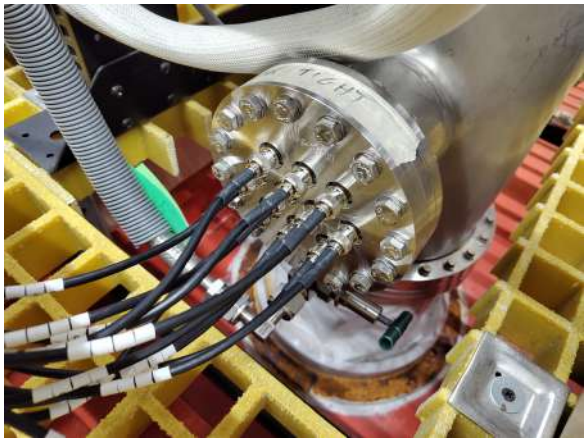

Figure 5: *Picture of new WL-195N cables connected to the flange of one of the chimneys on the top of ICARUS West module.*

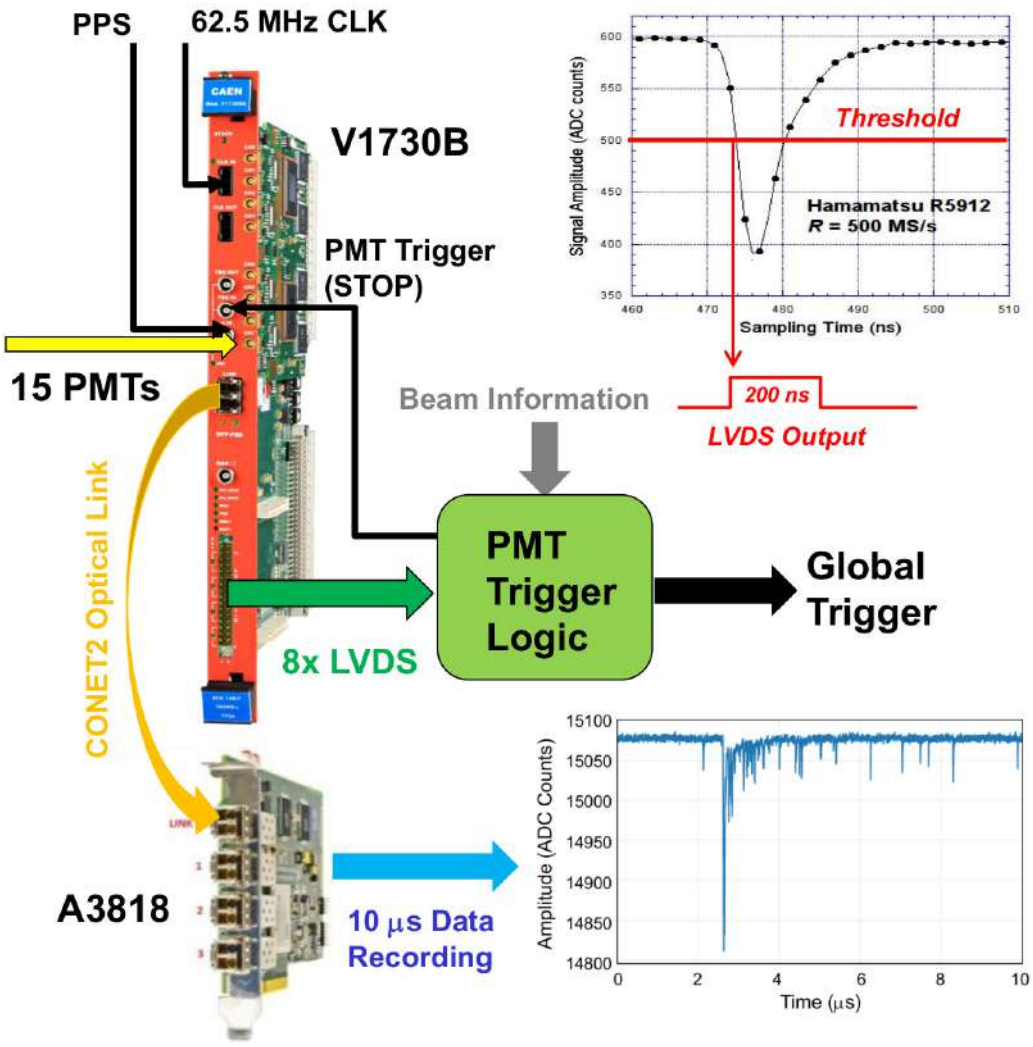

Figure 6: *Light detection system electronic setup. It is worth to point out that the 15 incoming PMT signals are the ones coming from the adder outputs. Also, PPS stands for GPS Pulse Per Second signal, and it is sent to all boards to keep them synchronised [7].*

tion system is shown in *Figure 4*. Each PMT is connected to a supply coaxial cable and to a signal coaxial cable. The power supply cables are connected to 8 CAEN A7030 boards that can provide up to 3 kV. The signal cables are connected to the signal processing electronics, located in an alcove by the detector. Both cables have a section inside the detector, connecting the PMTs to the chimneys, and a section outside the detector, connecting the electronics to the cables inside the chimneys by flanges on their surface. The section inside the detector is 7 m long and it consists in RG316/U signal cables and HTC-50-1-1 powersupply cables. The supply cables outside the detector are 37 m long RG58/U cables, connected to the flanges by means of SHV-SHV connectors. The signal cables outside the detector on the other hand were 37 m long RG/316U cables connected to the flanges by means of BNC-BNC connectors [5, 6]. In August 2023 the outside signal cables corresponding to the 180 PMTs in the West cryostat were replaced by new 28 m long WL-195N cables (in *Figure 5*; the undersigned contributed to the cable replacement). This replacement was carried out because a deterioration of the signal introduced by the cables was found out observing the shape of the signal pulse at the flange and at the end of the cables using an oscilloscope. The performance

of these new cables and their comparison with the old cables is discussed in the following *Section 5*.

4 PMT electronics

PMT electronics is designed to allow continuous read-out, digitization and independent waveform recording of signals coming from the 360 PMTs of the light detection system. The core of the electronic system that accomplishes this task is the ensemble of 24 V1730B digitizers stored into 8 VME crates, 6 boards for each TPC. Each board is a 16-channel 14-bit 500 MSa/s FLASH ADC having 2 Vpp input dynamic range. 15 of these channels are used in each board for the acquisition of the PMT signals, and each channel has 1024 consecutive buffers that can store 5 kSa corresponding to 10 μs. The data stream is circularly written in the active buffer until the board receives an external trigger pulse, which freezes the active buffer and moves the writing process to the next buffer. The data stored in the frozen buffer is read out by dedicated CONET2 optical links by means of CAEN V3818 PCI boards.

The signal cables coming from the PMTs are first connected to 24 custom made adder boards, each having 15 available channels, that have the task to generate a Low Voltage Differential Signals (LVDS) which is used in the triggering system of the detector, by summing a small fraction of the signals (5%) incoming in each channel. The rest of the signal is sent out from each channel into a corresponding channel of the digitizer which records the signal. Additionally the digitizers send out LVDS in 8 channels in terms of OR of 7 two-by-two adjacent input channels plus a single channel. All of these LVDS are processed by FPGAs together with other inputs, which can send out PMT trigger signals to freeze the digitizer memory buffers and store the data and global trigger signals.

The FPGAs evaluates if there is a minimal number of PMTs detecting a signal over a threshold (majority rule) or if the LVDS coming from the adder is over a threshold. This means that the detector trigger activates only if the light detection system sees sufficient light, either in number of activated PMTs or in detected photon quantity [7, 8]. *Figure 6* shows a scheme of how the electronics work.

5 Cable performance comparison

This section presents the results of the analysis of the data to compare the performance between the two signal cables, RG316/U and WL-195N. The analysis is mainly focused on the 180 PMTs of the West cryostat where the swap of the cables took place.

5.1 Waveform comparison

The data analysed in this subsection consists of two distinct laser run datasets, in other terms data of laser pulse signals detected by the detector PMTs and recorded by the digitizer boards. One of them was collected before the swap of the signal cables and the other one was collected after it. The averages of the various quantities were calculated considering 1000 events of the same run dataset, so although there is still room to determine the precise values including more events in the analysis, the statistics should be enough to give a rough but reliable estimate of the considered quantities. A sample laser pulse waveform is shown in *Figure 7*. It must be underlined that both the signals were flipped and aligned at the startpoint of the waveforms for comparison purposes. It is visibly possible to see that the new signal has a taller peak with respect to the old one. But this variation must be studied over a number of signals over many PMTs and quantified into numbers.

The variation of the signal shape could be quantified by several physical quantities. The most direct approach is the comparison of the peak amplitudes of the signals. Observing the plots in *Figure 8* it is clear that the amplitude

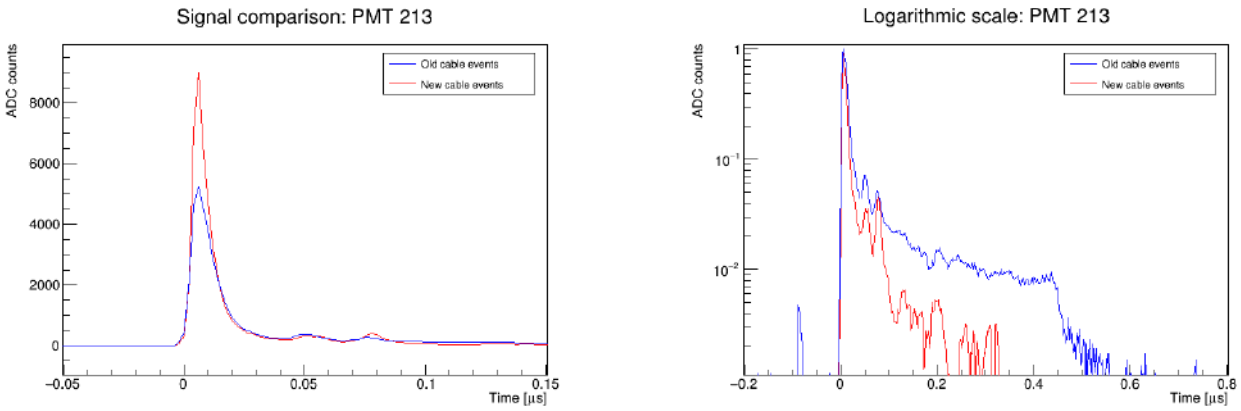

(a) (b)

Figure 7: *Comparison of an old cable signal waveform with a new cable one from the same PMT, aligned at their startpoint along the x axis and flipped along the y axis (7a); plot of the same waveforms normalised to the unity and on a logarithmic scale (7b).*

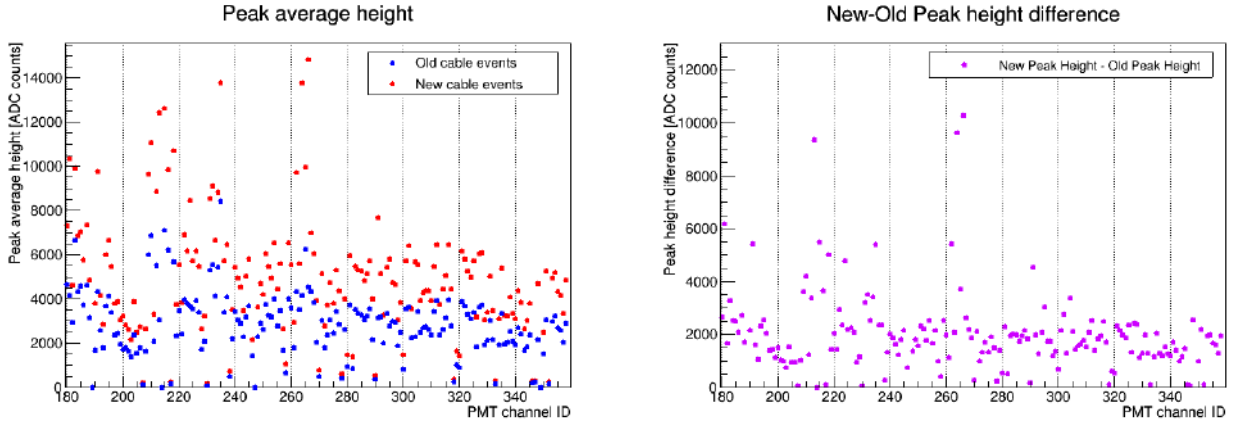

(a) (b)

Figure 8: *Plot showing the average signal amplitude over 1000 events in every PMT channel of the West cryostat before and after the cable swap (8a); the difference between the values of the new cables and the old cables in the 8a plot (8b).*

of the signal increased in every single PMT channel, therefore it is possible to confirm that the new cable does indeed increase the amplitude of the signal. The average increase percentage of the amplitude can be obtained by a gaussian fit of the distribution of the single increase percentages shown in *Figure 9b*, yielding a result of (60 ± 3) % increase on average of the signal amplitude.

A different quantity that can determine the improvement of the signal shape is the charge distribution along the waveform, more precisely the integral of the tail of the waveform over the integral of the entire waveform. In fact a signal is the variation of an electric voltage, which is proportional to the flowing current according to Ohm's law, which is the derivative of the moving charge quantity over the time. Thus the integral of the signal is proportional to the charge therefore the number of electrons reaching the digitizer. The tail of the integral refers to the time window between 80 ns and 1 μs after the startpoint of the waveform, where the startpoint is the timing at which the signal

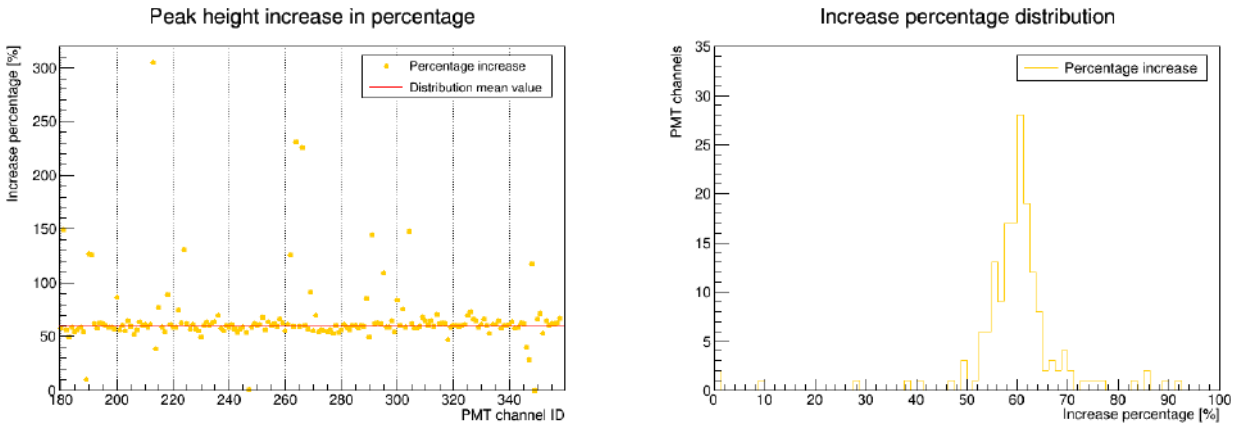

(a) (b)

Figure 9: *Increase percentage of the signal amplitude in every PMT channel of the West cryostat comparing the two cables (9a); the distribution of the values in the 9a plot (9b).*

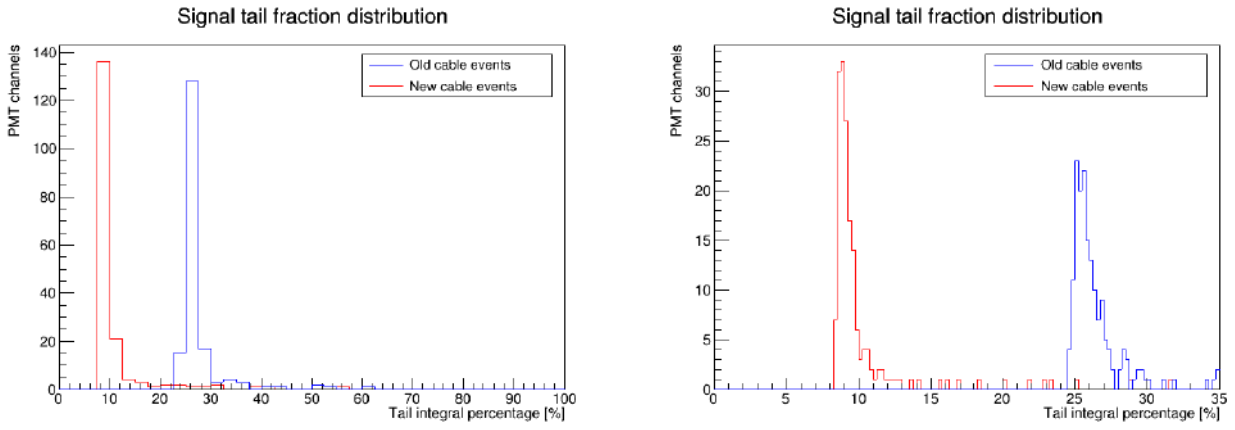

(a) (b)

Figure 10: *Distribution of the average tail integral fraction over 1000 events for every PMT (10a) and detail of the same distribution (10b).*

first reaches 10% of the maximum amplitude. This tail integral fraction is connected to the shape of the waveform since having a low value implies having a high charge concentration in the first few tens of ns of the signal, therefore a higher and narrower peak.

Figure 10 shows the distribution of the tail integral fractions measured in the different PMTs. Applying a gaussian fit to the two distributions it results that the tail integral of the signal was reduced from an average (25.6 ± 0.6) % on the old cables to (8.9 ± 0.3) % on the new cables. Once again, this tells that the signal waveforms collected using the new WL-195N cables have a larger amplitude and a smaller width of the pulse compared to the old RG316/U cable waveforms, implying a better timing resolution of the signal therefore an improvement in the timing resolution of the light calibration system.

5.2 Risetime Comparison

The risetime refers to the time window between the timings at which the waveform reaches 10% and 90% of its maximum amplitude. The variation of the risetime of the signal in the two cables could theoretically be measured by com-

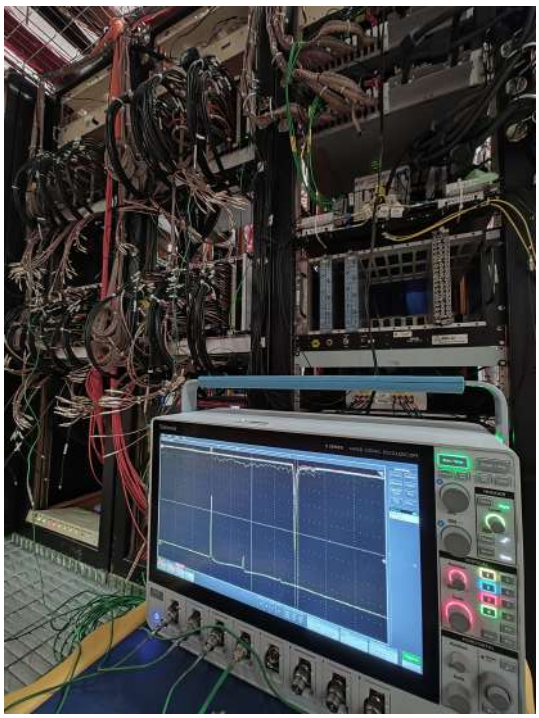

Figure 11: *Picture of an oscilloscope connected to the ICARUS PMT electronics showing a laser pulse signal detected by three different PMTs.*

paring the waveform of a laser pulse signal before and after the cable swap in the same PMT channel while applying the same supply voltage to the considered PMTs, as in the previous subsection. Unfortunately the risetime of the signal is a very small time window which cannot be measured precisely using the digitizer because of its not small enough sampling time of 2 ns. Therefore the data was collected by means of an oscilloscope having a sampling time of 160 ps, connecting it to the adder output channels of 3 previously chosen PMTs and triggering the signals directly with the laser pulse coming from the laser diode as shown in *Figure 11*. Firstly 500 signal waveforms were collected using the already installed new WL-195N cables, then the signal cables of the involved channels were temporarily switched back to the old RG316/U cables to collect additional 500 waveforms. The PMTs were chosen depending on the average amplitude of their signals (obtained in *Figure 8a*) and their channel location on the adder board for physical convenience. The precise risetime of the signals were determined as the difference of the precise timings at which the signal reaches 90% and 10% of its maximum amplitude, where the precise timings were calculated using a linear relation between the amplitudes at the timings right before and right after the threshold. *Figure 12* shows the distribution of the risetime for 500 signals using the old cable and the new cable. It is clear that the risetime of the new cables is overall smaller than the old cables one no matter what the amplitude of the signal is. By applying a gaussian fit to the distributions it is possible to obtain an average risetime for each PMT-cable combination, reported in *Table 1*. It is not possible to estimate a precise relation between the amplitude of the signal and the variation of the risetime of the signal simply because only three PMTs and signal amplitudes were considered. Additional waveforms from other PMTs would be necessary to have a more precise relation between the two quantities.
Additionally, the signal risetime of the new cables after a first equalisation of the PMT gains was considered too. In mid September 2023 a first approximate equalisation of the gain of the PMTs was carried out adjusting the sup-

	RG316/U risetime	**WL-195N risetime**	**Difference**
PMT 128 (Large)	(4.5 ± 0.1) ns	(3.9 ± 0.1) ns	(-11.8 ± 0.7) %
PMT 5 (Medium)	(4.0 ± 0.1) ns	(3.56 ± 0.08) ns	(-12.2 ± 0.5) %
PMT 158 (Small)	(4.2 ± 0.2) ns	(3.6 ± 0.1) ns	(-13.0 ± 0.8) %

Table 1: *Table summarising the results of the analysis of the two risetime distributions in the various amplitude cases.*

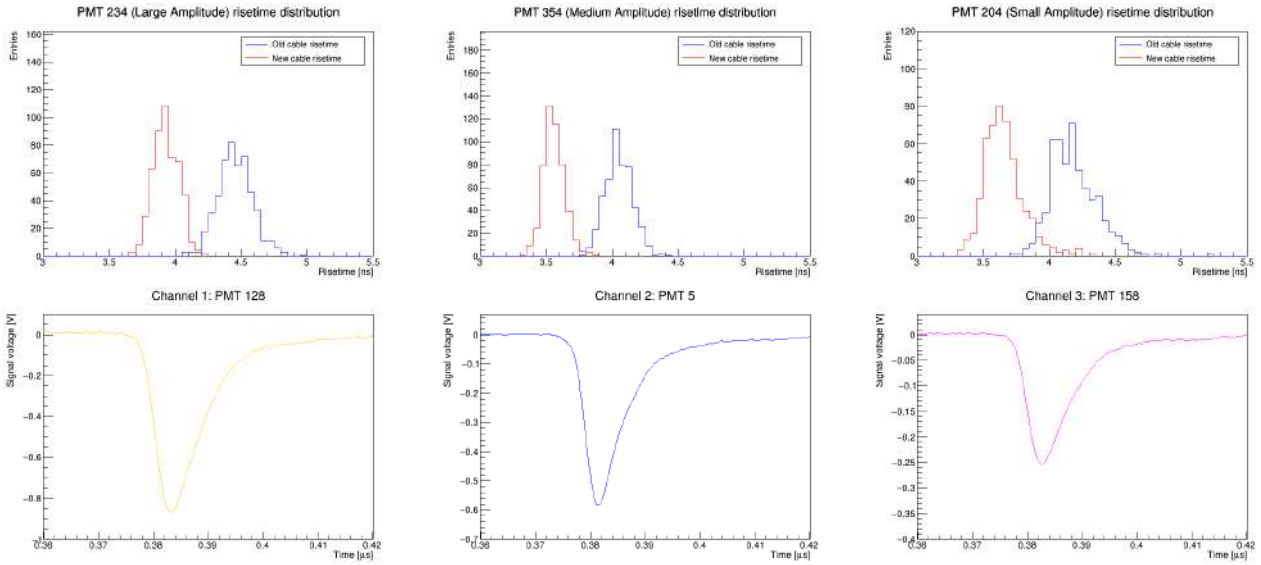

(a) (b) (c)

Figure 12: *Distribution of the risetime of 500 laser pulses measured using the old cables and 500 pulses using the new cables with corresponding new cable pulse samples. PMT 128 has signals with a large amplitude (12a), PMT 5 with a medium amplitude (12b) and PMT 158 with a small amplitude (12c).*

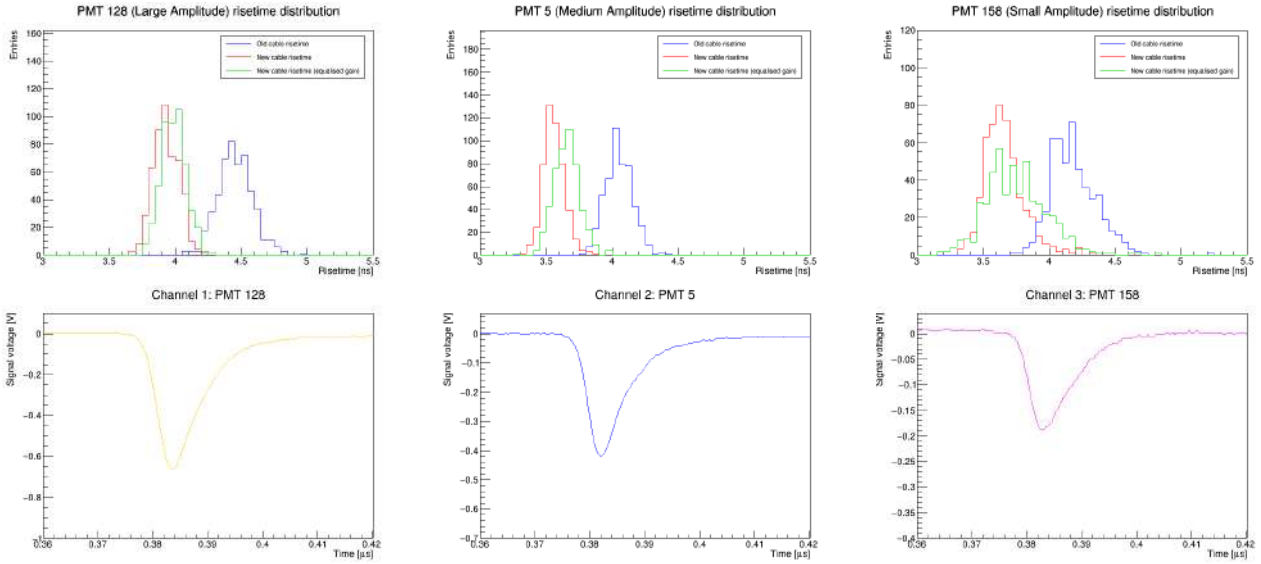

(a) (b) (c)

Figure 13: *Distributions shown in Figure 12 integrated with the distribution of 500 laser pulse signal risetimes measured using the new cables after the equalisation of the PMT gains, with corresponding pulse signal samples. PMT 128 has signals with a large amplitude (13a), PMT 5 with a medium amplitude (13b) and PMT 158 with a small amplitude (13c). In every PMT channel the amplitude of the signal is smaller compared to the non-equalised case.*

	WL-195N risetime before equalisation	**WL-195N risetime after equalisation**	**Compatibility**
PMT 128 (Large)	(3.9 ± 0.1) ns	(3.99 ± 0.09) ns	0.43σ
PMT 5 (Medium)	(3.56 ± 0.08) ns	(3.7 ± 0.1) ns	0.79σ
PMT 158 (Small)	(3.6 ± 0.1) ns	(3.7 ± 0.2) ns	0.42σ

Table 2: *Table comparing the results of the analysis of the two risetime distributions before and after the equalisation of the gains of the PMTs.*

ply voltages. After this change 500 waveforms were collected using an oscilloscope similarly to the previous steps, and the obtained data was compared with the results obtained with the new cable data previous to the equalisation of the gain. The result is shown in *Figure 13*. Firstly, the amplitude of the signal of every PMT is smaller compared to before the equalisation. However the amplitudes are far from equal among each other as an "equalisation" would lead to think. It is reminded though that the PMT gains are calibrated around interaction events occurring inside the TPC such as cosmic events, and not only based on the laser pulses of the calibration system, which can only measure gain differences on the same channel. In fact several optical fibers are misaligned and not directly pointing towards the PMT, therefore the power of the laser hitting the PMTs is not the same and only the variation of the amplitude could be considered for equalisation purposes. Looking at the distribution of the risetimes and applying once again gaussian fits, it is possible to see that the mean risetime of the signals slightly decreased compared to before. In particular the distribution of the small amplitude channel looks much more dispersed than before, having signal events with risetimes much off the mean value, in particular on the large side. One of the reasons that could be thought of this phenomenon is the fact that the amplitude of the signal is small at the point that the fluctuations of the baseline have a bigger impact on the shape of the waveform and the calculation of the waveform. *Figure 14* shows 2 wave-

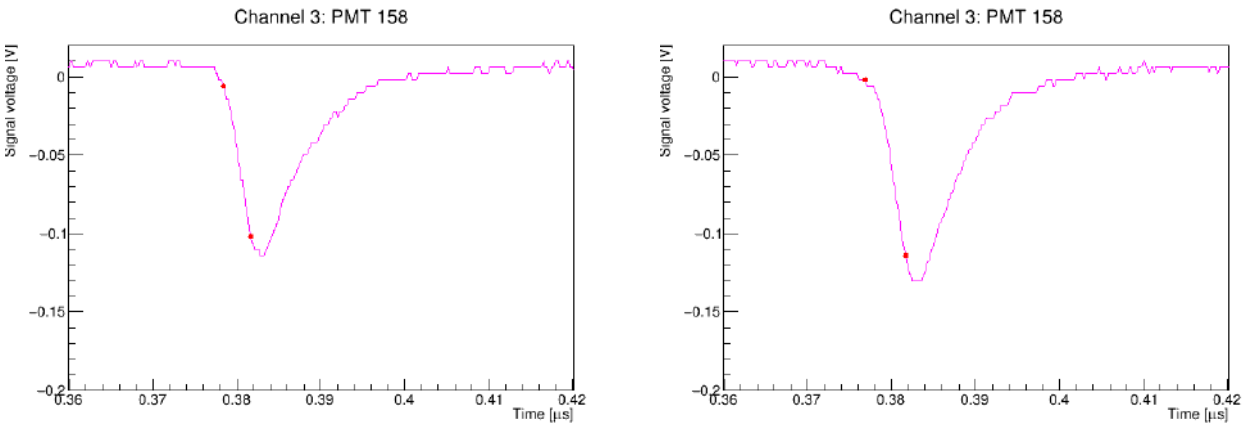

(a) (b)

Figure 14: *Two PMT 158 channel sample waveforms on the opposite sides of the risetime distribution with risetime startpoint and endpoint marked on the waveform; the plot on the left (14a) shows a waveform having low risetime (3.2 ns), while the one on the right (14b) has a high risetime (4.8 ns).*

forms from the post-equalisation dataset having small and large risetimes compared to the mean value of the distribution. It is possible to see that even if the two waveforms have a very similar shape, there is a difference in the amplitude of the signal right before the beginning of the pulse: one of them suddenly spikes up from the baseline and the other one gradually increases before going up substantially. The large difference in risetimes comes from the fact that the algorithm chooses as startpoint a point on the slope before the spike depending on the shape of the waveform, resulting in a variable risetime value. The results of the gaussian fit of the new distributions are shown in *Table 2*. As the previous case a higher statistic could lead to a result with a better precision, but even this data is enough to be able to say that the risetime values of the new signal cables before and after the PMT gain equalisation are compatible between each other, and that the slight adjustment of the PMT gains does not drastically affect the risetime of the signal in the new cables.

6 Conclusions

The change of the 180 signal cables of the West module of the ICARUS T600 detector, carried out in August 2023 replacing the old RG316/U 37 m long cables with new WL-195N 28 m long cables, lead to an improvement in the transmission of the signals from the PMTs to the data processing electronics. Analysing and comparing laser run data obtained using the laser calibration system before and after the swap of the cables, it was observed that the signal amplitude increased by (60 ± 3) % on average and that the integral of the tail of the waveform dropped from (25.6 ± 0.6) % to (8.9 ± 0.3) % of the entire waveform integral, implying a waveform that is larger in amplitude and shorter in time, leading overall to a better defined signal having a better resolution. In addition, it was also observed that the risetime of the signals were reduced between 11 and 13 % compared to before, and that a slight variation in the gain of the PMTs, which could be necessary for an equalisation of the gains moving from the current values, does not lead to a significant variation of its value.
The change of the cables in the East cryostat is expected to be carried out in early October 2023. After an equalisation of the gains of all the PMTs to a proper value, the light detection system of the ICARUS detector would be ready to start taking data regularly using the neutrino beams.

Bibliography

[1] R. Acciarri et al. *A Proposal for a Three Detector Short-Baseline Neutrino Oscillation Program in the Fermilab Booster Neutrino Beam*. 2015. arXiv: 1503.01520 [physics.ins-det].

[2] The University of Chicago. URL: https://voices.uchicago.edu/neutrino/about/projects/.

[3] Fermi Research Alliance LLC. URL: https://sbn.fnal.gov/.

[4] Particle Data Group et al. "Review of Particle Physics". In: *Progress of Theoretical and Experimental Physics* 2022.8 (Aug. 2022), p. 083C01. ISSN: 2050-3911. DOI: 10.1093/ptep/ptac097. eprint: https://academic.oup.com/ptep/article-pdf/2022/8/083C01/49175539/ptac097.pdf. URL: https://doi.org/10.1093/ptep/ptac097.

[5] ICARUS Collaboration. *ICARUS at the Fermilab Short-Baseline Neutrino Program – Initial Operation*. 2023. arXiv: 2301.08634 [hep-ex].

[6] B. Ali-Mohammadzadeh et al. "Design and implementation of the new scintillation light detection system of ICARUS T600". In: *Journal of Instrumentation* 15.10 (Oct. 2020), T10007–T10007. DOI: 10.1088/1748-0221/15/10/t10007. URL: https://doi.org/10.1088%2F1748-0221%2F15%2F10%2Ft10007.

[7] W. Badgett et al. "The electronic set-up for the scintillation light detection system of ICARUS-SBN at Fermilab". In: *Nuclear Instruments and Methods in Physics Research Section A: Accelerators, Spectrometers, Detectors and Associated Equipment* 1047 (2023), p. 167871. ISSN: 0168-9002. DOI: https://doi.org/10.1016/j.nima.2022.167871. URL: https://www.sciencedirect.com/science/article/pii/S0168900222011639.

[8] M. Babicz et al. "The scintillation light detection system of ICARUS-T600: Hardware implementation and early results". In: *Nuclear Instruments and Methods in Physics Research Section A: Accelerators, Spectrometers, Detectors and Associated Equipment* 1046 (2023), p. 167685. ISSN: 0168-9002. DOI: https://doi.org/10.1016/j.nima.2022.167685. URL: https://www.sciencedirect.com/science/article/pii/S0168900222009779.